Instituto Superior Técnico

Computational Fluid Mechanics

HW3

Authors :
Diogo Carvalho Nº83677
José Santos Nº83704
Miguel Brito Nº83711
Gonçalo Oliveira Nº84256
Philip Widmaier Nº95467

Professors :
Prof. José Carlos Fernandes Pereira
Prof. José Manuel da Silva Chaves Ribeiro Pereira

December 22, 2019

Contents

1 Hypersonic Shock Boundary Layer Interaction

1.1 Boundary conditions

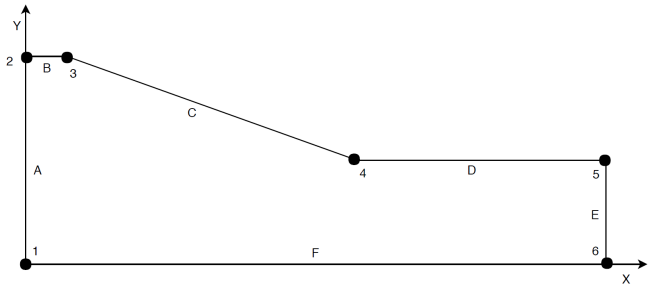

Figure 1: Esquema da geometria em estudo

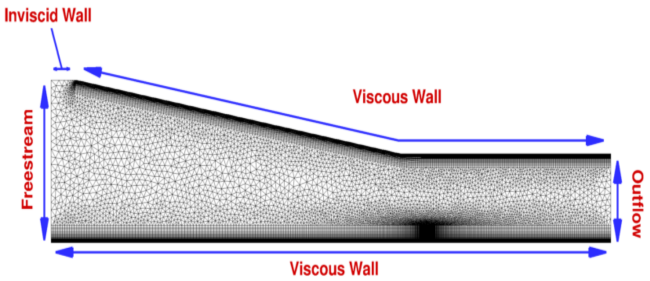

Figure 2: Malha e condições fronteira usado no caso da NASA

We will explore this problem from two different starting points, first one is the assumptions made by NASA in their case study and the other one, is to try and reproduce as closely as possible the conditions used in the experimentation process presented in Schulein. In figure 2 we can see the the boundary conditions chosen by NASA with all walls having a fixed temperature of 300K, while in the experiment, there were only two walls, the plate "F" which is a viscous wall, with prescribed temperature, 300K, and a shock generator plate "C", also a viscous wall but adiabatic, all the remaining boundaries are free streams.

In the inlet section, "A" in figure 1, we have a free stream with the horizontal direction, flowing towards "A" this flow has prescribed stagnation temperature, stagnation pressure and Mach number, all free streams have these static conditions as flow parameters, however only on "A" will the flow have the horizontal direction needed for the conditions to be used by the software.

$$\text{Stagnation temperature} : T_{0A} = 738^{o}R = 410K$$
$$\text{Stagnation pressure} : p_{0A} = 307.84psi = 2.12MP_a$$
$$\text{Mach number} : M_A = 5$$

However, *Star-CCM+* uses static conditions for free stream so in order to convert these initial conditions, we use the following isentropic equations:

$$\frac{T_0}{T} = 1 + \frac{\gamma - 1}{2} M^2 \qquad \frac{p_0}{p} = (1 + \frac{\gamma - 1}{2} M^2)^{\frac{\gamma}{\gamma - 1}}$$

1.2 Mesh design

For the process of the mesh design to start, it is important to fully understand the extent of the *Optical Skin Friction Measurements in Short-duration Facilities*. The objective of the experiment is to analyse the interaction between the boundary layer development and the shock wave. Since it is required to use a mesh with around 30.000 cells, it is really important to know the regions that need to be refined and the base size of the elements to be reduced.

1.2.1 Prism layers

Due to the fact that Dirichlet boundary conditions are used in the bottom wall, not only for velocity (no-slip condition) but also for temperature, temperature and velocity boundary layers are developed. For this reason, prism layer local refinement are applied in the wall region. The higher gradients intensity require a more accurate discretization that both the cell base size reduction and the local alignment of the gradients, flow and normal of the face of the cells, will provide. Combining the facts that the turbulent boundary layers have a high value of thickness and the discretization near the wall requiring more accuracy, a stretching factor of 1.15 is used. This way, the efficiency of the prism layer is improved without causing excessive variations from one cell to the other.

1.2.2 Refinement of interest regions

There are areas where the flow properties are almost constant and thus, these areas won't require the same analytical precision as the regions where field properties are changing abruptly. For instance, in the region where the shock is developed one has to take extra care while designing the mesh. Knowing the exact location of the shock wave, it is possible to reduce the elements size in order to improve the accuracy of the calculations. The location of the shock is calculated based on shock expansion theory.

$$tan(\beta) = 2cot(\theta)\frac{M_1^2 sin^2(\theta) - 1}{M_1^2(\gamma + cos(2\theta) + 2}$$

For a deflection angle of the shock generator of 14^o the values obtained were:

$$\begin{cases} \theta_1 = 23.3^o \\ M_2 = 3.5941 \\ \theta_2 = 13.7^o \end{cases}$$

The mesh was refined in the shock and reflected shock regions and comparisons were made with not refined meshes. It was possible to verify, for instance, the decrease in the length of the parameters variation (shock region). This decrease, approximates the solution to the discontinuity expected, improving the final result. A line probe was created, perpendicular to the shock wave, in order to verify this phenomena and the Mach number variation is plotted in the next figure. On the left a non-refined mesh was used with around 6.000 cells, and in the right the final mesh (refined and with prism layers) with around 30.000 cells.

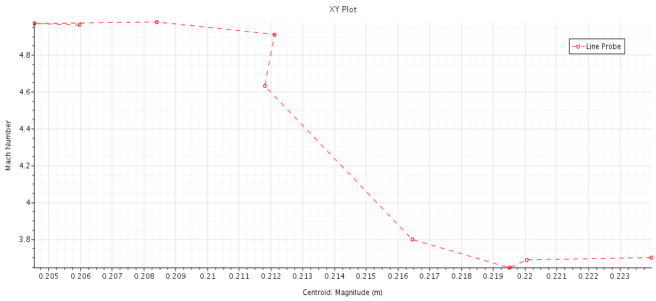

Figure 3: Polygonal non-refined mesh

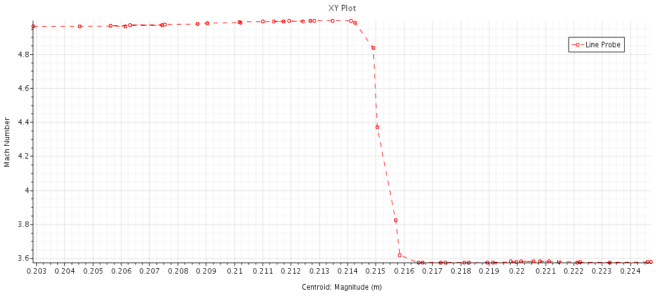

Figure 4: Polygonal refined mesh

1.3 Final mesh

After defining the criteria followed to design the mesh, the final mesh used is presented in 14. It can be noticed that prism layers were only used in the bottom wall since it is there that the shock/boundary layer interference occurs. This way, decreasing the number of cells used to cover the top wall, the refinement on the interest areas can be improved.

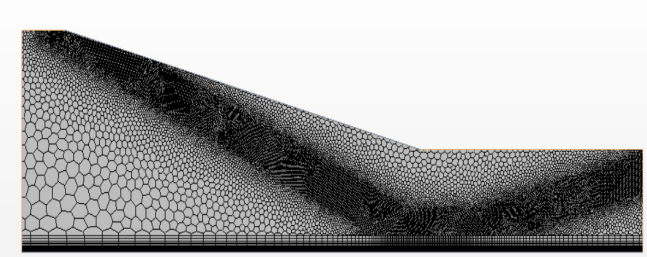

Figure 5: Mesh final

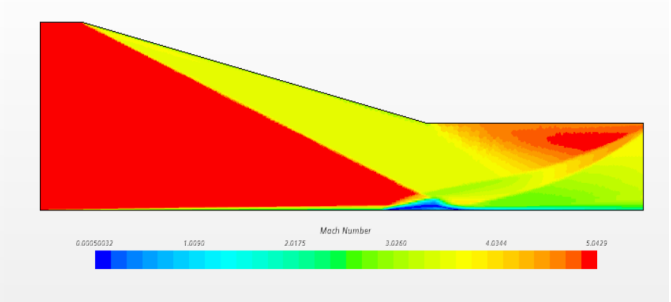

Figure 6: Resultado final com modelo SST

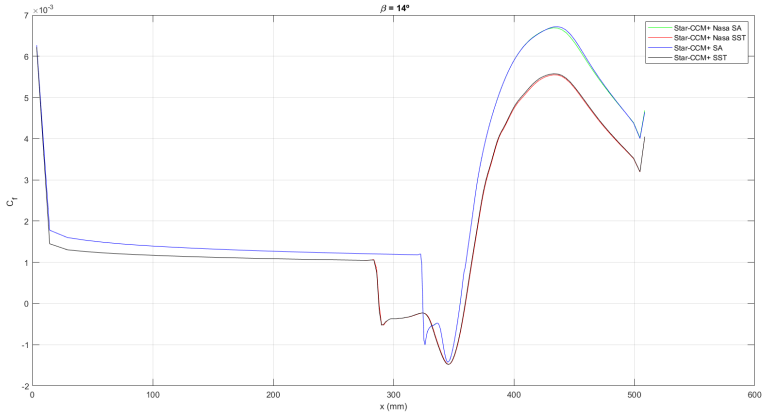

Figure 7: Mesh comparison

As we can see the different boundary conditions, applied in the NASA verification, did not overly influence the result of the simulation as seen in figure 16. The differences between the simulations with the true conditions of the experiment and the ones used by NASA are minimal, we can assume that this is because the different assumptions are made on plates far from our region of interest, the boundary layer and the shock-boundary layer interaction. We can however, from the same figure 16 observe the effect that the turbulence models have on the final solution, with the Menter's Shear Stress Transport (SST) model predicting a much larger area of separation compared to the Spalart-Allmaras (SA).

1.4 Comparison with experimental results

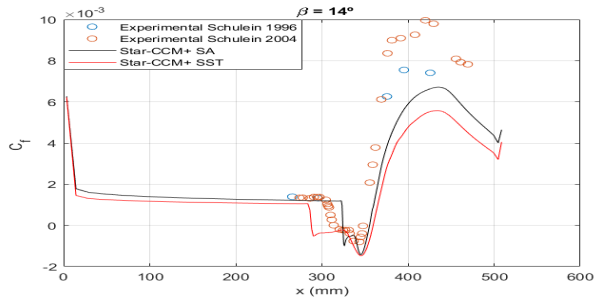

Figure 8: Skin Friction Coefficient

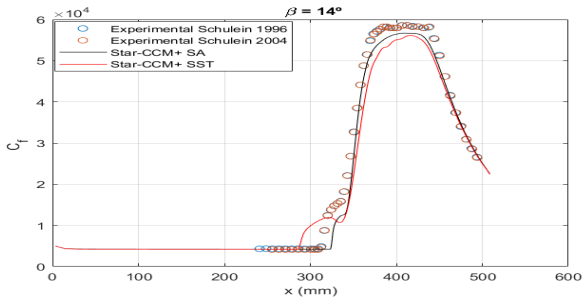

Figure 9: Pressure

Firstly, looking at the skin friction coefficient, figure 8 we can see that both the experimental results from the two sets of data from Shchulein in 1996 and 2004, and from Star-CCM using both turbulent models, are all quite different from each other. This should make us weary of our simulation results, but also of the experimental data. Skin friction is calculated on the experiments using models, therefore we cannot be certain that the results are accurate, or what is the scale of the experimental errors. This is one of the reasons why we also compare the static pressure at the bottom wall, "F" on figure 1, because pressure is not calculated but measured by sensors in the Schulein experiments.

There is a clear difference in the skin friction coefficient between both models, with SST predicting a much larger separation bubble than SA, which seems to be more accurate comparing with the experimental data, which can be seen in table 1. SST also predicts a smaller overall skin friction which corresponds with the NASA data, and therefore, gives us confidence in our results. Looking at figure 8 we can also see that SA model follows more accuratelly the data from the Schulein experiments, around the separation zone, while after separation none of the models corresponds to data taken from the papers.

	S(m)	R(m)	Bubble Size (m)
Schulein 2004	0.314	0.348	0.034
SA	0.324	0.355	0.031
SST	0.288	0.3595	0.071

Table 1: Separation and Re-attachment of the "separation" bubble

Analyzing the pressure at the wall, shown in figure 9 we can now see that our simulation results are more similar to the experimental ones and, as we have seen before, this is a sign that the numerical results are quite good because pressure is a more viable quality reference than skin friction. Despite this, the computated pressure by Star-CCM is still lower than experimental results, in most of the region, with results being not as clear near the separation point. In both the pressure and skin friction results, we can see that SA model has a better performance than SST. This could be theoretically expected since SA model was developed in order to solve flow between walls, and SST is more directed towards inside boundary layer flow and non-disturbed flow.

To further understand the difference between both turbulence models, we computed the absolute error between the numerical results and the experimentation results for both the skin friction, figure10, and pressure, figure 11, data. The experimental data used was the one from Schulein 2004,simply because it has more points of data than the earlier experiment. Since two sets of data will not be found at the same

coordinates in x, an interpolation was made, which will add some error to our results, in order to compare as evenly as possible the different sets of data.

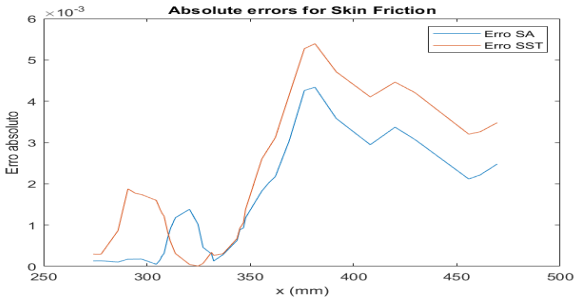

Figure 10: Skin Friction Coefficient

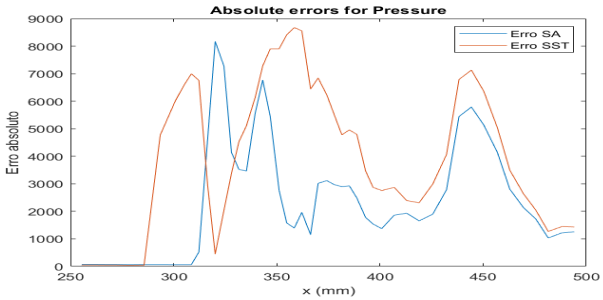

Figure 11: Pressure

These results confirm our previous assessment that the SA model is overall better for this case study, especially looking at figure 10, whereas in figure 11 it is harder to observe the difference between the modules due to the higher range of results.

1.4.1 Mach at sections 7,8 and 9

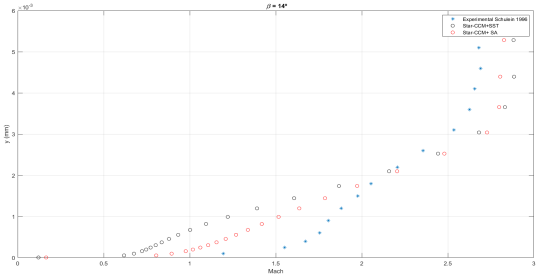

Figure 12: Mach number variation at section 7

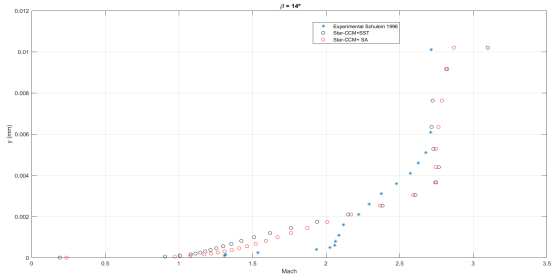

Figure 13: Mach number variation at section 8

In the Schulein 1996 experiment, data was collected at nine different sections positioned alongside the bottom plate, where we are studying the boundary layer. The ones chosen to compare were sections 7, 8 and 9, which are all placed after the separation area. Inside the boundary layer there is a considerable discrepancy between Mach number values, with both the experimental results by Schulein and CFD analyses presenting a linear relation, but with different slopes. Outside the boundary layer there is also an increase in the Mach number for the CFD results obtained. For section 8 the discrepancy between the linear relation between Mach number and distance increases and the SST and SA methods show similar results. Following analyses of figure 12 one can conclude that the method that shows fitter values when comparing with experimental results is the SA turbulence method, which agrees with the assessment made earlier.

In order to analyse the Mach error comparing Schulein (1996) results and the CFD simulations realized, a simple MATLAB code was developed. This code approximates the experimental results in order to compare values in the exact location of the sensors placement. This way, it is possible to obtain the absolute error and understand in which distance to the wall the error is higher and also if the velocity is being underestimated or overestimated. The error is calculated only by subtracting the obtained Mach

number to the Schulein Mach number. It is once again possible to realise that the chosen method has a bigger impact closest to the separation zone. In all three sections there is an underestimate of the Mach number closest to the wall, with the SST method having the higher error values of around 0.8, almost a full order of magnitude. Due to the proximity of the wall and the number of cells considered, it was not possible to obtain the small slope value. Decreasing the distance between cells would be a possible way to solve this issue, however, the number of cells near the wall is already sufficiently small, and decreasing it even more could result in the loss of information between cells. As the distance to the wall increases the error decays until an overestimate of the Mach number is reached, showing an oscillation pattern. The lowest error values are obtained for the region outside the boundary layer as expected.

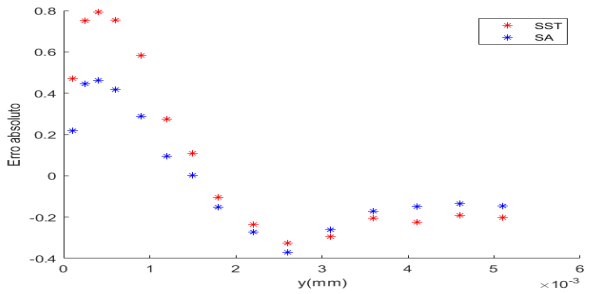

Figure 14: Absolute error (section 7)

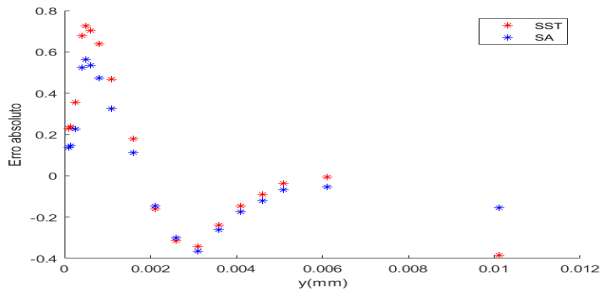

Figure 15: Absolute error (section 8)

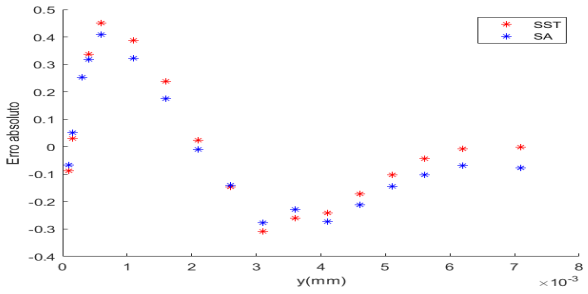

Figure 16: Absolute error (section 9)

	max(Abs.Error)	max(Rel.Error)	Mean Error(Abs.)
SST	0.79	0.48	0.37
SA	0.46	0.29	0.23

Table 2: Absolute and relative errors for SST and SA methods for section 7

2 Sod's Shock Tube - 1D

Gary Sod's shock tube problem is considered. For this simulation we use a 1D domain with a length of 20m. Our mesh consists of N=320 cells with a $\Delta x = 0.0625m$. Firstly, we analyze the differences between the use of a segregated and a coupled solver. In these simulations a second-order implicit time scheme is employed with a time step $\Delta t = 0.0001s$. Secondly, we compare the solutions obtained between three coupled solvers with an explicit time scheme. Then, the influence of the number of cells is evaluated for first and second order implicit time schemes.

2.1 Segregated/Coupled Flow

Solving the continuity, momentum and energy equations can be performed with two main different options. On one hand, we can solve these equations independently of each other. This is done by a segregated solver and because the matrix in the linear system of equations only takes into account each equation at a time, the memory required is small. On the other hand, we can solve all equations at the same time. This, of course leads, to a much larger matrix (NxN larger) in the linear system of equations. In turn, to store and solve the solution we need a lot more memory in comparison to the previous option. One might think that the segregated option is always better because it requires less memory however the coupled algorithm usually yields more robust and accurate solutions, particularly in the presence of shock waves. In this section, we compare a coupled solver (Roe FDS) and three different segregated solvers (Segregated Fluid Isothermal, Segregated Fluid Temperature and Segregated Fluid Enthalpy).
Segregated Fluid Isothermal treats temperature as a constant across the continuum. It is a good choice when temperature variations are negligible. Assuming a constant field of temperature, obviously leads to a smaller computational effort, since we are not solving the energy transport equation. The other two segregated Fluid solvers work similarly. The difference is the Segregated Fluid Enthalpy treats enthalpy as the variable in the equation transport equation, while the Segregated Fluid Temperature treats temperature as the variable in the equation transport equation. Although, the recommendation is to use the former when there is combustion and the latter when there is not, both solvers render extremely similar solutions for this problem.

2.1.1 First-order spatial discretization scheme

First-order convection schemes display high numerical diffusion. This can be seen in all four boundaries of interest. Contrary to the theoretical expectations, for this order of convection scheme, the segregated solver deals with the shock wave better than the coupled solver. The latter displays enough diffusion to remove the oscillations from the second-order time scheme, while the former does not, where an oscillation appears near the shock wave. Due to the dissipative nature of both schemes, the discontinuities in head and tail of the expansion wave have a large effect in the neighboring cells. Furthermore, the coupled flow expansion wave is leading the segregated flow. All have trouble with the discontinuity surface. In the analytic solution matter and heat diffusion is not considered. Nonetheless, the numerical solvers do take into account these effects and in addition to the numerical diffusive property of a low order spatial discretization scheme, the solution obtained smooths the transition across fluids.
Regarding the Segregated Isothermal Fluid solver, across all the simulations, we see that only the pressure ratios across both the shock and expansion waves are accurately calculated. However, we can get a very crude approximation of both their position, as well as the velocity and density variations across them. On the other hand, the discontinuity surface is not taken into account and the average of both fluids density is assumed in the region between the shock and expansion waves. Finally, the temperature field gives no information, due to explanation already mentioned of assuming a constant temperature field.

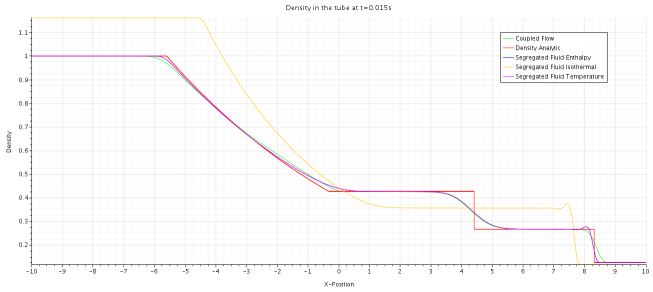

(a) Density in the tube at t=0.015s

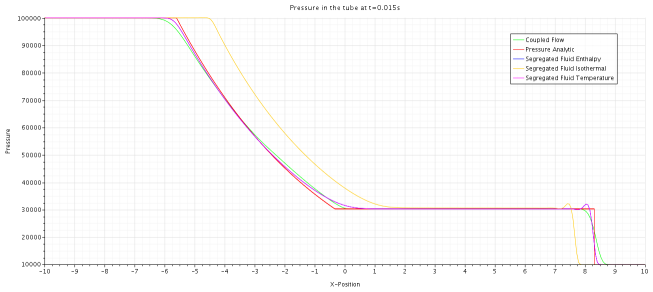

(b) Pressure in the tube at t=0.015s

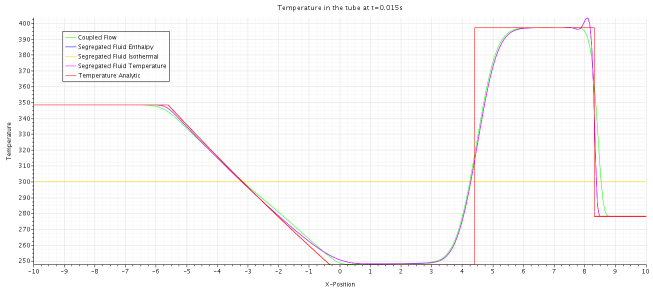

(c) Temperature in the tube at t=0.015s

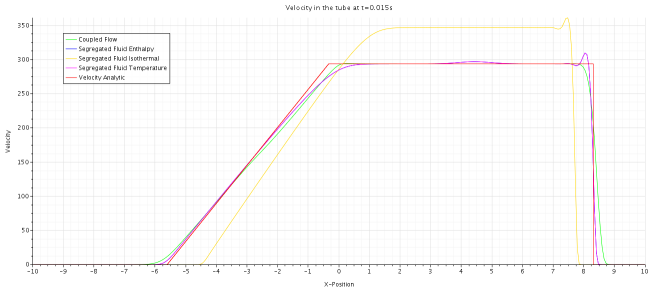

(d) Velocity in the tube at t=0.015s

Figure 17: First-order spatial scheme

2.1.2 Second-order spatial discretization scheme

As we increase the order of discretization, the numerical diffusion also diminishes. Using a second-order convection scheme with either a coupled or segregated solver we obtain a solution extremely close to the analytic. In contrast to the lower order convection scheme, the positions of the head and tail of the expansion wave are almost identical to the analytic values. Furthermore, the surface between the fluids is better defined. This time around, we have introduced an oscillatory behavior prior to shock wave in the coupled flow algorithm's solution. This, however, is an acceptable condition having in mind the increase in accuracy compared to the first-order convection scheme.

2.1.3 Third-order spatial discretization scheme

Increasing the order to a third-order convection scheme does not lead to a better scheme. This scheme has insufficient dissipation and spurious oscillations now also appear in the discontinuity between the fluids and increase near the shock wave. This does not come with a much better representation of the discontinuity when put against the second-order convection scheme.
We have seen that both the use of a segregated flow solver that takes into account the energy transport equation or a coupled flow solver sided with a second-order spatial discretization scheme leads to the most accurate with less oscillatory behavior between these options. We will now discuss the influence of different coupled solvers together with an explicit and implicit time scheme.

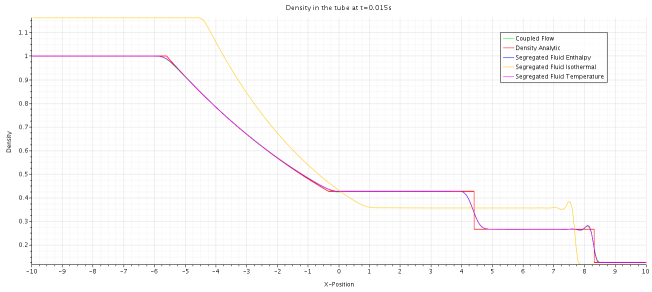

(a) Density in the tube at t=0.015s

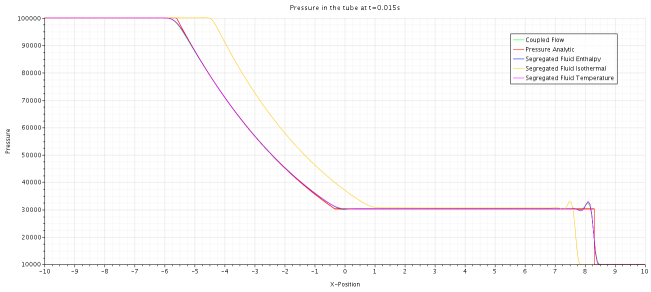

(b) Pressure in the tube at t=0.015s

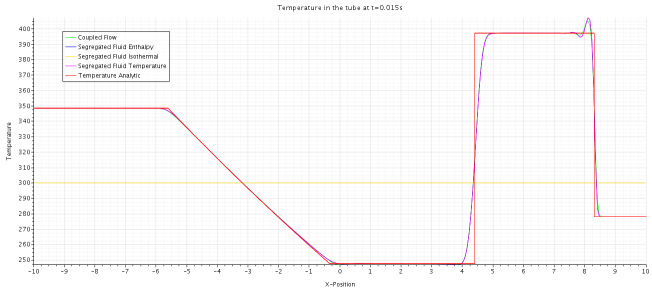

(c) Temperature in the tube at t=0.015s

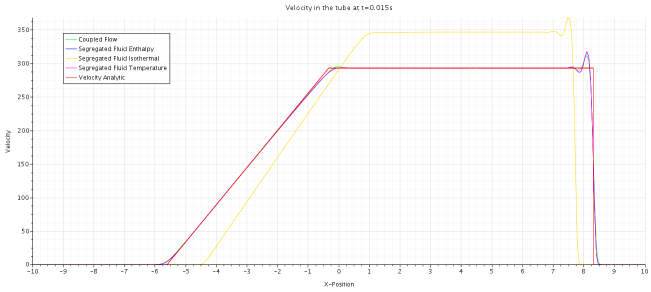

(d) Velocity in the tube at t=0.015s

Figure 18: Second-order spatial scheme

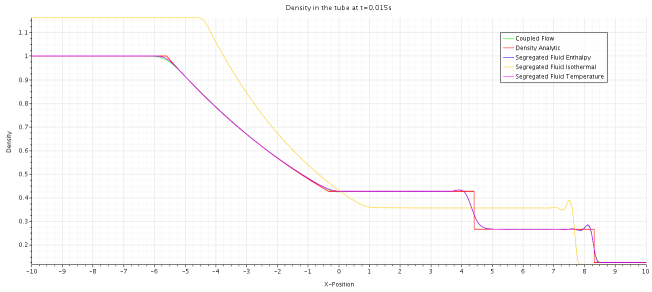

(a) Density in the tube at t=0.015s

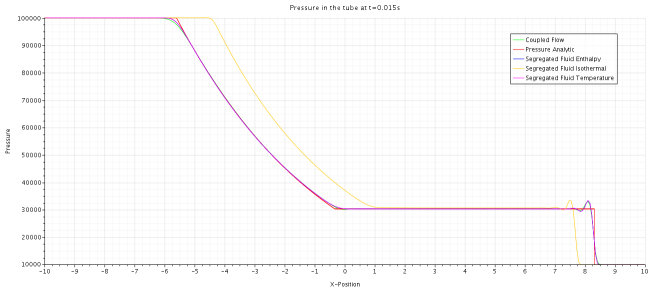

(b) Pressure in the tube at t=0.015s

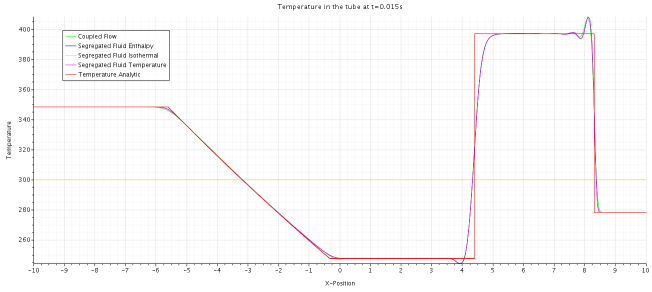

(c) Temperature in the tube at t=0.015s

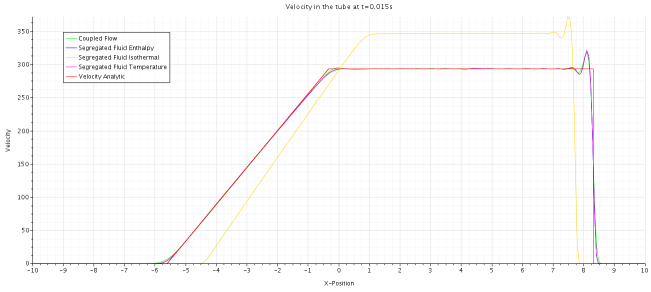

(d) Velocity in the tube at t=0.015s

Figure 19: Third-order spatial scheme

2.2 Explicit Time Scheme

For this discussion we will use a second-order spatial discretization scheme for the reasons stated in the previous section. The comparison is made between a flux vector splitting method (AUSM+ FVS) and a flux difference splitting method (Roe FDS). We also use the Roe FDS method where there is no blending to obtain the pressure difference at the flux interface. However, because this is done only at the incompressible limit, we should expect no difference between both Roe FDS methods since we are working with compressible flow. In this simulation we used a Courant number C=1.

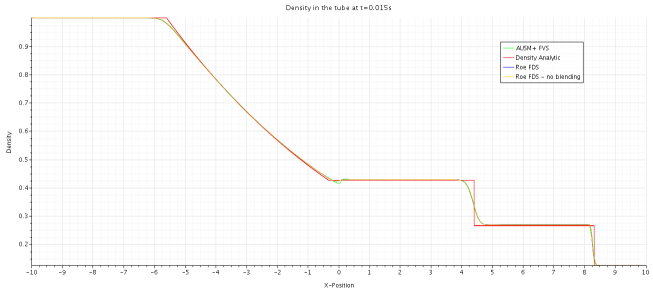

(a) Density in the tube at t=0.015s

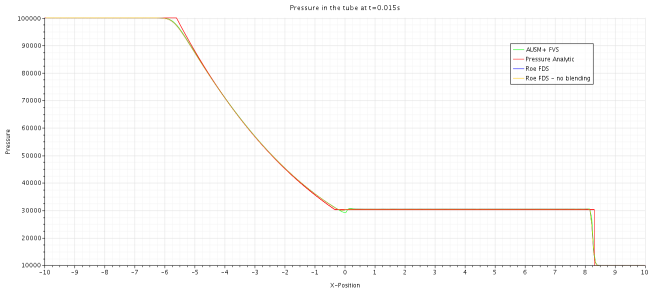

(b) Pressure in the tube at t=0.015s

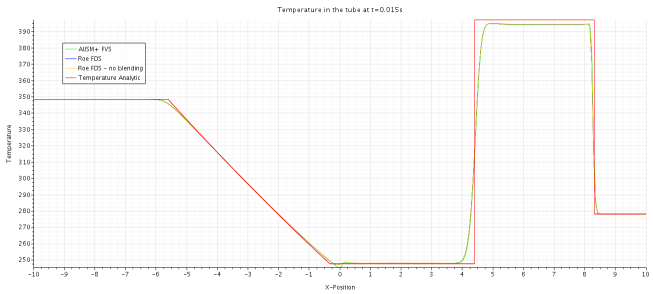

(c) Temperature in the tube at t=0.015s

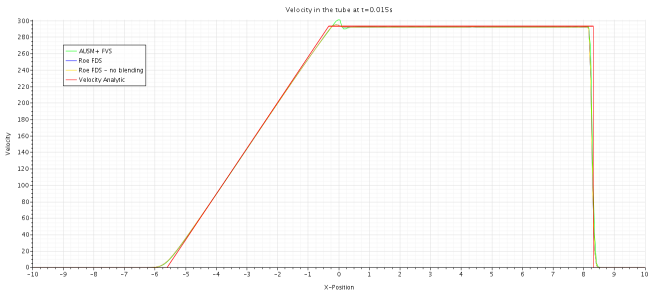

(d) Velocity in the tube at t=0.015s

Figure 20: Explicit time scheme

As stated before, we see no difference between blending and no blending in the Roe solver. The FDS and FVS are also similar with the exception of an oscillation in the tail of the expansion wave. The shock wave in the numerical solution lags compared to the analytic solution. In the temperature field, the temperature after the shock wave passes has an error of 3K. This contrasts with the previous implicit solution where no error was obtained. This means that the explicit time scheme leads to errors in the energy equation in the presence of a shock wave. Finally, all other values are obtained with a very good approximation to the analytic values.

2.3 Implicit Time Scheme

For this discussion is used a first and second order implicit time scheme with Roe FDS, where the impact of cell number variation is evaluated. The problem was simulated for 320, 160, 80 and 40 cells, producing the following pressure and temperature plots where results can be compared also with the exact solutions.

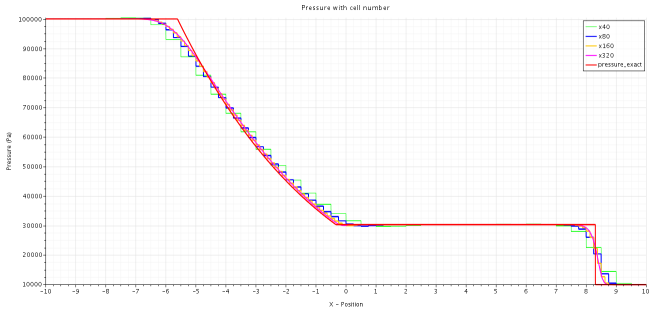

(a) Pressure in the tube at t=0.015s for different cell number

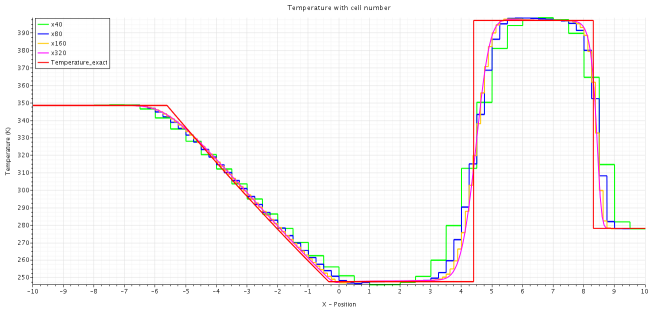

(b) Temperature in the tube at t=0.015s for different cell number, 1^{st} order time scheme

Figure 21: 1^{st} order time scheme

As expected, a less refined discretization of the tube leads to larger errors. It can be seen that results are notably worse where properties vary abruptly, like at the head and tail of the expansion and at the shock wave regions.

Having a lower number of cells means the cell size Δx will increase. With this increase, a larger portion of tube will be modelled by a single cell. For example, the largest cell number here used was 320, which means $\Delta x = 20/320 = 0.0625m$, while the lowest was 40, which makes $\Delta x = 0.5m$.

This huge difference in cell size, has great influence and is visible in the regions aforementioned. Cells show larger errors and for a larger extent of the tube, meaning that there is more error propagation to neighbouring cells with bigger cells.

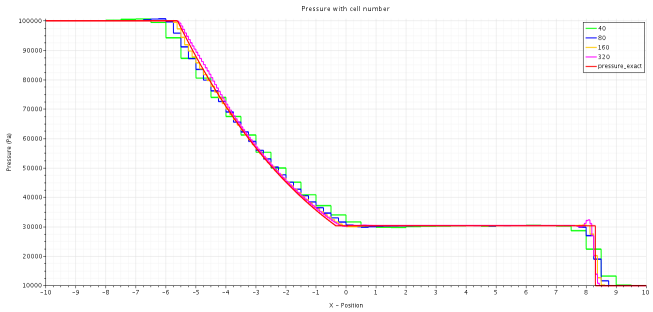

(a) Pressure in the tube at t=0.015s for different cell number

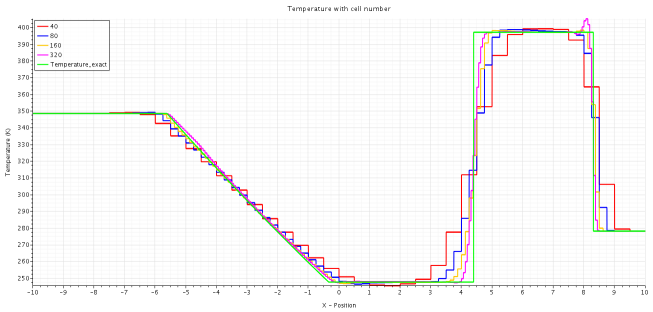

(b) Temperature in the tube at t=0.015s for different cell number

Figure 22: 2^{nd} order time scheme

Comparing the order of time schemes, it can be seen that first order produces similar results for small number of cells, but improves a lot for larger numbers. It is also worth noting that computation time increases with the number of cells, as well as with the time scheme, as implicit time scheme require more computational effort than the explicit. Both factors must be taken into consideration when performing simulations where high accuracy is desired and computational resources are limited.